EDF
Electricité de France

Direction des Etudes et Recherches

SERVICE ENSEMBLES DE PRODUCTION
Département Machines

SERVICE APPLICATIONS DE L'ELECTRICITE ET ENVIRONNEMENT
Département Laboratoire National d'Hydraulique

Décembre 1993

BARON F.
CARUSO A.
DUPLEX J.
LEFEVRE L.

EXTENSION DES ALGORITHMES POUR ECOULEMENTS INCOMPRESSIBLES AUX ECOULEMENTS COMPRESSIBLES : VALIDATION SUR UNE MAQUETTE DE VANNE REGULATRICE

EXTENSION OF INCOMPRESSIBLE ALGORITHMS TO COMPRESSIBLE FLOWS : VALIDATION ON A GOVERNING VALVE MOCK UP

Pages : 00011

95NB00017

Diffusion : J.-M. Lecœuvre
EDF-DER
Service IPN. Département SID
1, avenue du Général-de-Gaulle
92141 Clamart Cedex

ISSN 1161-0611

SYNTHÈSE :

La puissance des turboalternateurs des réacteurs à eau pressurisée est contrôlée par des vannes régulatrices placées à l'admission de la turbine haute pression. On présente dans cette note une comparaison entre les mesures relevées dans une maquette 2D de vanne régulatrice et une simulation numérique de l'écoulement.

Afin de prédire et de simuler les écoulements transsoniques à faible Mach, on présente une nouvelle extension de deux codes initialement dédiés aux écoulements incompressibles et instationnaires (méthode elliptique).

Ces codes utilisent soit la méthode des différences finies, soit, pour les géoémtries complexes, la méthode des éléments finis. La prédiction de ces types d'écoulements est difficile, d'une part en raison du fort couplage qui existe entre les phénomènes physiques tels que la turbulence, et d'autre part en raison de la complexité de la géométrie. La comparaison des résultats numériques avec des mesures de pression et des strioscopies confirme la validité de cette approche. Les résultats indiquent clairement que cette méthode saisit correctement la structure du jet.

EXECUTIVE SUMMARY :

The capacity of turbogenerators in PWR is regulated with governing valves located at the admission of the high-pressure turbine. In this paper we present a comparison between measurements and a numerical simulation of the flow in a 2D mock up of this governing valve.

To predict and simulate transonic flow at low Mach numbers, we present a new extension of two codes initially devoted to incompressible and unsteady flows (pressure based method).

The codes use either Finite Difference Method or, for complex geometry, Finite Element Method. Predicting those kinds of flows is difficult due to strong coupling between physical phenomena like turbulence on one hand, and the complexity of industrial geometry on the other hand. The comparison of numerical results with pressure measurements and also with schlieren photographs confirms the validation of this approach. The results show clearly how the method correctly captures the structure of the jet.

Extension of incompressible algorithms to compressible flows : validation on a governing valve mock-up.

F. Baron, A. Caruso, J. Duplex, L. Lefèvre
Electricité de France, Direction des Etudes et Recherches,
6 quai Watier, 78401 Chatou Cedex, France

1 - INTRODUCTION

In a nuclear power plant, the capacity of turbogenerators in PWR is regulated with governing valves located at the admission of the high-pressure turbine. The condition created in these valves (due to throttling of steam) involves generation of jet structures, possibly supersonic ones. These valves consist of a moving part that changes the cross-section of the fluid path. Since the upstream conditions (pressure and temperature) are relatively constant, the mass flow rate, and hence the capacity of turbogenerators, can be controlled.

Operating under partial load is obtained by stream-throttling which means dissipating a considerable quantity of energy. Such volumes of energy constitute a potential risk for the mechanical integrity of the equipment. Studies performed on units featuring typical geometry (figure 1) have demonstrated the following flow path particularities [1] :

- Coanda effect : the jet reattaches on the convex solid surface
- Separation : as the expansion ratio increases, the jet creates a recirculation zone behind the separation point
- Reattachment : for high expansion ratio the jet can reattach on the opposite wall
- Shock : the presence of separation and reattachment yields shocks.

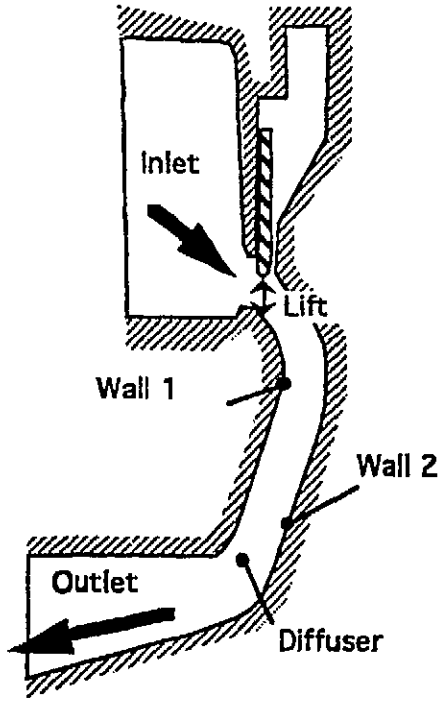

Figure 1. Description of the valve

Because of those flowpath particularities experimental results of a 2D mock up of this governing valves (static pressure and schlieren photograph) have been used to validate the new extensions of incompressible codes to transonic flow.

2- DESCRIPTION OF THE MODELS

The following numerical procedure derives from the fractional step algorithm proposed by Chorin [3] which already takes into account density variations. Several improvements have been implemented [4] and will be presented in this chapter. The Navier-Stokes and scalar equations are solved in the same way, using a quasi-unsteady time marching algorithm.

Turbulence effects are taken into account by a coupled and implicited k-ε model [5,6] written in terms of time increments. This model minimises the number of unrealistic negative values and avoids numerical instabilities [7].

2 - 1 Basic equations

Instantaneous equations are ensemble averaged, written in terms of Favre average defined as (The ~ symbol is relative to the Favre averaged quantities while the - symbol is relative to the Reynolds average) :

$$\widetilde{G} = \frac{\overline{\rho G}}{\overline{\rho}} \text{ with } \overline{G(t)} = \lim_{N\to\infty} \frac{1}{N}\sum_{n=1}^{N} G_n(t) \quad (1)$$

where G(t) is the instantaneous value of G. Thus, the Favre-averaged equations for velocity vector $\widetilde{U}$ and enthalpy $\widetilde{H}$ are :

Mass conservation equation :

$$\frac{\partial \overline{\rho}}{\partial t} + \mathrm{div}\,(\overline{\rho}\,\widetilde{U}) = 0 \quad (2)$$

Transport equation for mean velocity :

$$\overline{\rho}.\left(\frac{\partial \widetilde{U}}{\partial t} + \widetilde{U}.\vec{\nabla}\widetilde{U}\right) = -\vec{\nabla}\overline{P} - \nabla.\tau \quad (3)$$

where $\tau = (\mu + \mu_t).\left(\nabla\widetilde{U} + \nabla^t\widetilde{U} - \frac{2}{3}(\nabla.\widetilde{U}).I\right) - \frac{2}{3}\overline{\rho}\widetilde{k}.I$

Transport equation for mean enthalpy :

$$\overline{\rho}\frac{\partial \widetilde{H}}{\partial t} + \overline{\rho}.\widetilde{U}.\vec{\nabla}\widetilde{H} = \left(\frac{\partial \overline{P}}{\partial t} + \widetilde{U}\vec{\nabla}\overline{P}\right) + \nabla.\left(\frac{\lambda}{C_p}\nabla.H\right) + S_H \quad (4)$$

where μ_t and σ_t are respectively the turbulent viscosity and turbulent Prandtl number ; H is the enthalpy per unit of mass.

2 - 2 Turbulence model

The standard k-ε model is used for turbulence. The transport equations of k (mean turbulent kinetic energy) and ε (its mean dissipation rate) are :

$$\overline{\rho}.\left(\frac{\partial \widetilde{k}}{\partial t} + \widetilde{U}\,\vec{\nabla}\widetilde{k}\right) = \mathrm{div}\left[\left(\mu + \frac{\mu_t}{\sigma_k}\right)\vec{\nabla}\widetilde{k}\right] + \widetilde{P} + \widetilde{G} - \overline{\rho}\,\widetilde{\varepsilon} \quad (5)$$

$$\overline{\rho}.\left(\frac{\partial \widetilde{\varepsilon}}{\partial t} + \widetilde{U}\,\vec{\nabla}\widetilde{\varepsilon}\right) = \mathrm{div}\left[\left(\mu + \frac{\mu_t}{\sigma_\varepsilon}\right)\vec{\nabla}\widetilde{\varepsilon}\right] + c_{\varepsilon 1}\frac{\widetilde{\varepsilon}}{\widetilde{k}}\left(\widetilde{P} + \widetilde{G}\right) - c_{\varepsilon 2}\,\overline{\rho}\,\frac{\widetilde{\varepsilon}^2}{\widetilde{k}} \quad (6)$$

where $\widetilde{P}$ is the production rate defined as :

$$\widetilde{P} = 2\mu_t\,\mathrm{tr}\left[\left(\vec{\nabla}U + \vec{\nabla}{}^t U\right)^2\right] - \frac{2}{3}\overline{\rho}\,\widetilde{k}\,\mathrm{div}(\widetilde{U}) - \frac{2}{3}\mu_t(\mathrm{div}(\widetilde{U}))^2 \quad (7)$$

and $\widetilde{G}$ the contribution of buoyancy is written as :

$$\widetilde{G} = \frac{\mu_t}{\sigma_t}\vec{\nabla}\overline{P}\,\vec{\nabla}\overline{\rho} \quad (8)$$

The turbulent viscosity is defined as :

$$\mu_t = C_\mu\,\overline{\rho}\,\frac{\widetilde{k}^2}{\widetilde{\varepsilon}} \quad (9)$$

The constants of the model are (e.g. Launder and Spalding [5], and Launder [6]) :

σ_t	σ_ε	σ_k	C_μ	$C_{\varepsilon 1}$	$C_{\varepsilon 2}$
0.7	1.3	1.	0.09	1.44	1.92

2 - 3 Wall effects

For boundary conditions, the main difficulty is to take into account the wall effects. Indeed, the real boundary conditions of vanishing velocity cannot be applied for two reasons : on one hand, it would require a too fine mesh near the wall and on other hand, the standard k-ε model is no more valid in the viscous sublayer. The so-called wall functions are then necessary. The mesh boundary is supposed to be at distance y from the wall where the velocity profile is known. In practice, we use the standard logarithmic law [8], [9] :

$$\frac{u_w}{u*} = \frac{1}{K}\ln(y^+) + 5.2$$

where $y^+ = y\frac{u_*}{\nu}$, u* is the friction velocity linked to the friction stress σ* by $\sigma_* = -\rho u_*^2$ and K is Von *Karman*'s constant (K=0.41).

y^+ and u* are determined iteratively at each wall point for each time step. The corresponding boundary conditions for k and ε are: $k = \frac{u_*^2}{\sqrt{C_\mu}}$ and $\varepsilon = \frac{|u_*|^3}{Ky}$

3 - NUMERICAL TECHNIQUES

3 - 1 Quasi-unsteady algorithm

Transport equations (2) to (6) are solved using a quasi-unsteady algorithm where time discretization uses a first order scheme [8],[9] :

$$\rho\left[\frac{G^{n+1} - G^n}{\delta t} + U^n\,\vec{\nabla}G^n\right] = \mathrm{div}\,(K_G\,\vec{\nabla}G^{n+1}) + S_G \quad (11)$$

where δt is the time step, G^n and G^{n+1} are the values of G at the n th and (n+1) th time step. The rates of change for Favre averaged velocity, k, ε and scalar variables, after the advection step, are completed explicitly (explicit pressure gradient, explicit diffusion and source terms). In order to avoid instability, this explicit treatment is completed by an implicit integration of diffusion and source terms for the increments for all variables ; this treatment is coupled for k and ε. For steady flows computed as limit of a transient, all increments tend towards zero with convergence in time ; thus splitting approximations have little influence and solutions are fairly independent of the chosen time step.

The solution of (10) is divided into two parts :

3- 1 - 1 An advection step, solving

$$\frac{\hat{G} - G^n}{\delta t} + U^n \vec{\nabla} G^n = 0 \qquad (12)$$

The solution $\hat{G}$ is obtained using the characteristics methods [8] with quadratic interpolation allowing to minimise numerical diffusion : each particle trajectory passing by a node at time t_{n+1} is computed backwards in time, using a Runge-Kutta method, to time t_n where the transported quantities (U,H,k,ε) are interpolated on the finite element mesh:

$$\tilde{G}(\vec{x}) = G^n(\vec{x_c}) \text{ and } \vec{x_c} = \vec{x} - \int_{dt} \vec{u}\, dt \qquad (13)$$

3 - 1 -2 A diffusion step, solving

The diffusion step is resolved with a Eulerian implicit scheme.

$$\rho\left[\frac{G^{n+1} - \hat{G}}{\delta t}\right] = \text{div}\,(K_G \vec{\nabla} G^{n+1}) + S_G \qquad (14)$$

Once the advection step done, the set of equations (2) to (6) becomes :

$$\rho\left[\frac{U^{n+1} - \hat{U}}{\delta t}\right] = -\vec{\nabla} P^{n+1} + \text{div}\left[(\mu+\mu_t)\vec{\nabla} U^{n+1}\right] + \vec{S}_U \qquad (15)$$

$$\rho\left[\frac{k^{n+1} - \hat{k}}{\delta t}\right] = \text{div}\left[\left(\mu + \frac{\mu_t}{\sigma_k}\right)\vec{\nabla} k^{n+1}\right] + S_k^{n+1} \qquad (16)$$

$$\rho\left[\frac{\varepsilon^{n+1} - \hat{\varepsilon}}{\delta t}\right] = \text{div}\left[\left(\mu + \frac{\mu_t}{\sigma_\varepsilon}\right)\vec{\nabla} \varepsilon^{n+1}\right] + S_\varepsilon^{n+1} \qquad (17)$$

$$\rho\frac{\left[H^{n+1} - \hat{H}\right]}{\delta t} = \text{div}\left(\frac{\lambda}{C_p}\vec{\nabla}.H\right) + \frac{\partial P}{\partial t} + \theta\,\vec{U}\,\vec{\nabla P} + S_H^{n+1} \qquad (18)$$

3 - 1-3 Solutions of the systems

For the computation of the velocity a third step is required in order to satisfy the continuity condition. For this step the density will remain explicit at time t_n but density time variations are taken into account by linearisation [4] :

$$\boxed{\frac{d\rho}{dt} = \left[\frac{\partial \rho}{\partial p}\right]_h \frac{dp}{dt} + \left[\frac{\partial \rho}{\partial h}\right]_p \frac{dh}{dt}} \qquad (19)$$

- $\frac{dh}{dt}$ comes from equation (18) in which $\theta=0$ (prediction step) and will be updated after computation of P and U at time t_{n+1} with $\theta=1$.
- A state law (for example the perfect gas law : $\rho^n = \frac{P^n M}{RT^n}$) allows to close the system and to compute the partial derivatives $\frac{\partial \rho}{\partial p}$ and $\frac{\partial \rho}{\partial h}$.

Finally the continuity equation becomes :

$$\frac{1}{c^2}\frac{dp}{dt} + \text{div}(\rho U) = f_h \qquad (20)$$

where f_h is an explicit contribution of the enthalpy after diffusion step and c the speed of sound :

$$\frac{1}{c^2} = \left[\left(\frac{\partial \rho}{\partial P}\right)_H^n + \frac{1}{\rho}\left(\frac{\partial \rho}{\partial H}\right)_P^n\right] \qquad (21)$$

3 - 2 "Local time step" technique

For stationary problems, a "local time step" can be used into the previous equations to rapidly reach the steady state. The value of time step δt can be computed on each point of the mesh to have a local Courant number (based on advection velocity) of order 1. This technique is very useful when dealing with problems having simultaneously small zones at high velocity and large regions at low velocity (recirculations zones for example). In practice, at each point i, δt is computed by :

$$\delta t_i = \frac{C\, h_i}{u_i} \qquad (22)$$

where C is the Courant number, h_i a local size and u_i the velocity at point i.

4 - NUMERICAL RESULTS

Flow simulation inside the valve has been achieved for a constant lift and for different expansion ratios (e.r.$= \frac{P\ inlet}{P\ outlet}$). Experimental results show that for low expansion ratios (<3) the jet adheres to wall 1 (Fig. 17). Jet is then quasi subsonic or slightly supersonic. As soon as the expansion ratio is greater than 3, the jet separates from the wall 1 before re-attaching to the same wall downstream (Fig. 11). A recirculation zone (separation bubble) appears behind the separation point. For high expansion ratios (>4) the presence of the second wall prevents the jet from

expanding freely and causes the jet to reattach on the second wall with shocks patterns (Fig. 12).

The jet separation is due to the increase of pressure in the widening part after the valve. Pressure and viscous forces are then counter to the flow. Thickness of the boundary layer increases and friction stress is cancelled out at separation point.

First results have been obtained with the Finite Difference 3D code ESTET [9]. For high expansion ratios (>4) the global behaviour of the flow calculated by ESTET is in good accordance with flow visualisations and shows the ability of the method to represent a supersonic jet (see Fig. 7 to 10). The code predicts with accuracy the structure of the jet and its reattachment on the opposite wall. The comparisons with pressure measurements on the wall 1 (Fig. 1 to 2) show an accurate evaluation of the pressure depression close to the throat but an over-estimation downstream of the separation (the pressure calculated is greater than the one measured). In particular, for low expansion ratio, the code tends systematically to generate a jet separation which should only appear for an expansion ratio greater than 3.

Numerical prediction of separation point depends drastically on the mesh refinement close to the wall but it is difficult to have a local refinement with a structured grid, especially for the convex wall (Fig. 5 to 6). Actually some tests on a refined mesh have shown better agreements with experimental results but would have need to much CPU time to converge.

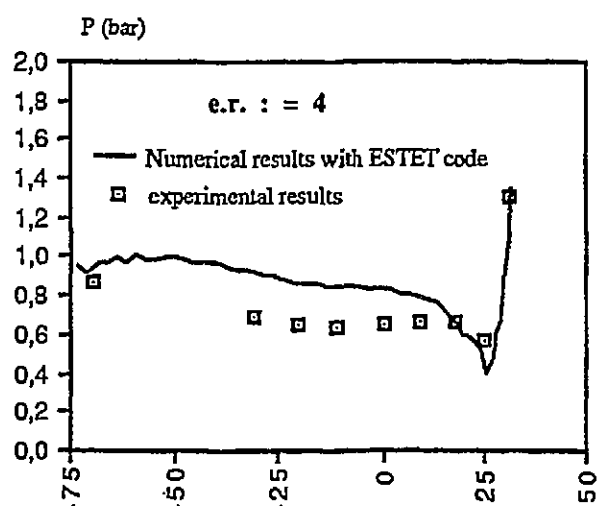

figure 1 : Static pressure on the wall for an e.r. = 4 with the FD code : ESTET

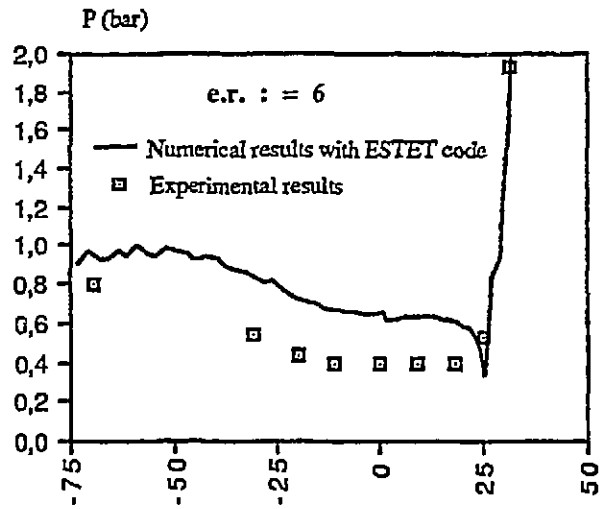

figure 2 : Static pressure on the wall for an e.r. = 6 with the FD code : ESTET

To confirm this assumption, the method has been extended to a 2D version of a non structured FEM code [10,11] which allows a better description of the throat (see Fig. 13). This code is a 2D prototype, in which the numerical algorithms are tested, before being implemented in a new compressible version of the 3D code N3S. At this moment only low expansion ratio without strong shocks have been performed. The FEM description of the throat gives then a better agreement with measurements (Fig. 3 to 4) and visualisations (Fig. 14 to 16). In particular the code is able to predict the complex structure of the jet with compression and depression zones on the wall without any separation of it. The validity of this second approach has now to be extended to larger expansion ratio leading to strong shocks and detach jet.

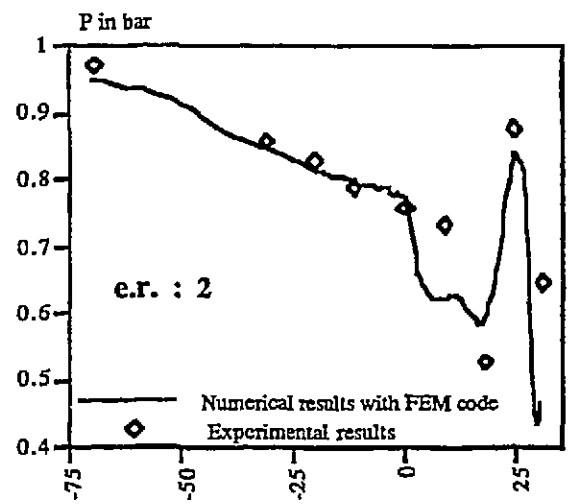

figure 3 : Static pressure on the wall for an e.r. =2 with the FEM code

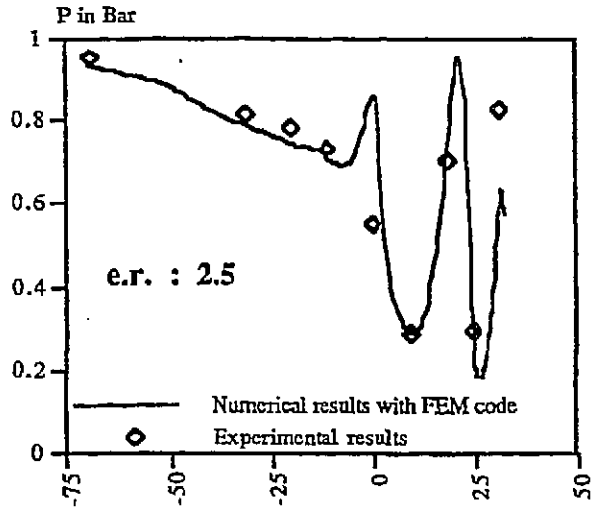

figure 4 : Static pressure on the wall for an e.r. =2.5 with the FEM code

5 - CONCLUSION

A numerical scheme to predict turbulent flow, based on either Finite Difference or Finite Element Method, and accurate treatment of the fractional step algorithm has been presented. It has been applied to a turbulent flow in a governing valve of turbogenerators in PWR.

Comparisons with a 2D mock up of this valve give very encouraging predictions. A "local time step" has proved to be very useful when one wishes to rapidly reach steady state in complex geometry.

The Finite differences approach has proved the capacity of the algorithm to represent a supersonic jet but has shown its limit to predict with accuracy an attached jet because of the poor description of the geometry. Better results have been obtained with a FEM code, which allows a good description of the throat and of the convex wall but this second approach needs now further developments to represent strong shocks.

6 - REFERENCES

[1] J.M. Richard - M. Pluviose
"Aerodynamic instabilities in governing valves of steam turbines" *proceedings of the institution of Mechanical Engineers*
Turbomachinery : latest Developments in a changing scene- C423/005

[2] J.M. Richard
"Calcul comparatifs d'écoulement dans une géométrie bidimensionnelle de maquette de soupape d'admission H.P. CP2" Note interne HP-43/90.20

[3] Chorin A.J.
'Numerical solutions of the Navier-Stokes equations', *Math. Comp.* 22, 745, 1968.

[4] Simonin O., Bechart J.
"Modélisation des écoulements compressibles"
rapport EDF-DER HE-44/89.12

[5] Launder B.E., Spalding D.B.,
'The numerical computation of turbulent flows', *Computer methods in applied mechanics and engineering*, 3 , 1974.

[6] Launder B.E., 'Turbulence transport models for numerical computation of complex turbulent flows', *Von Karman Institute for fluid dynamics*, lecture series 3, 1980.

[7] Simonin O., Viollet P.L.,
'Prediction of an oxygen droplet pulverization in a compressible subsonic coflowing hydrogen flow', *Symposium on Numerical Methods for Multiphase Flows*, Toronto, June 4-7, 1990.

[8] Chabard J.P., Metivet B., Pot G., Thomas B., 'An efficient finite element method for the computation of turbulent incompressible flows', *Hemisphere publishing corporation editor*, to appear.

[9] M.Gabillard, J.D. Mattei
Descriptif informatique du code ESTET- V3.0. Rapport EDF HE-44/90.13

[10] A. Caruso, N. Mechitoua
"Finite computation of turbulent diffusion flame"
rapport EDF-DER HE-44/92.20

[11] A. Caruso, N. Mechitoua, J. Duplex
"Modélisation des écoulements compressibles turbulents en maillage non structuré par extension des méthodes numériques appliquées aux écoulements incompressibles. Rapport d'avancement"
rapport EDF-DER HE-44/93.02

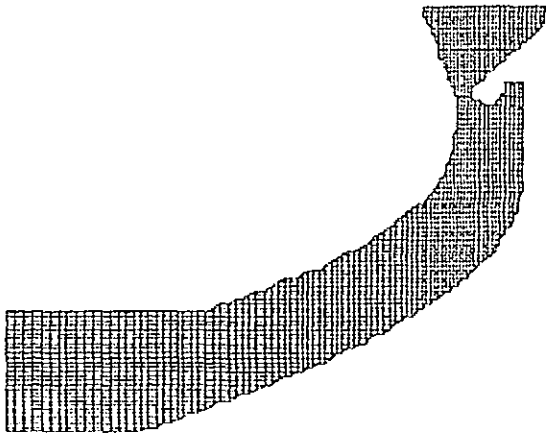

Fig 5 :Mesh of 27846 nodes

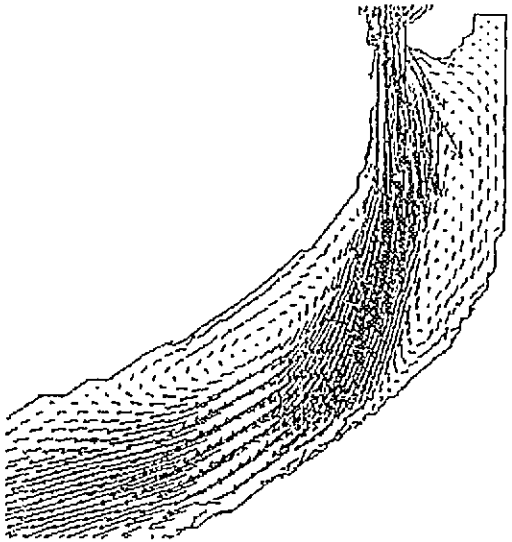

Fig7 : velocity (expansion rate=4)

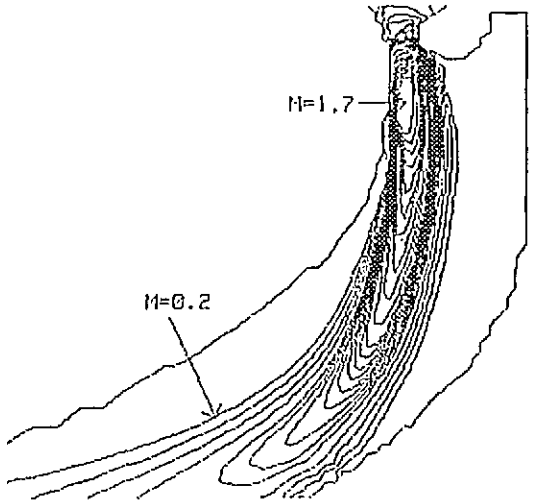

Fig 9 : Mach number (expansion rate=4)

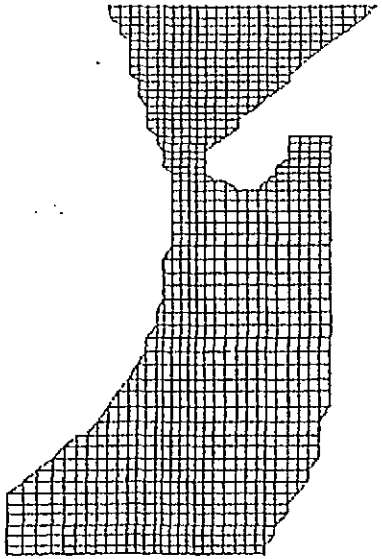

Fig 6 : Mesh vue near the throat

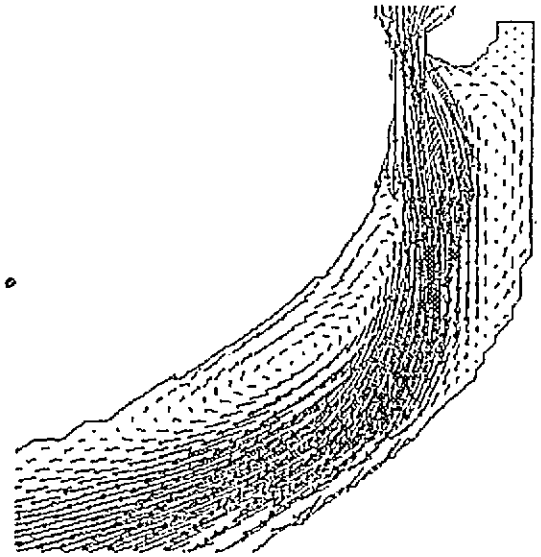

Fig 8 : velocity (expansion rate=6)

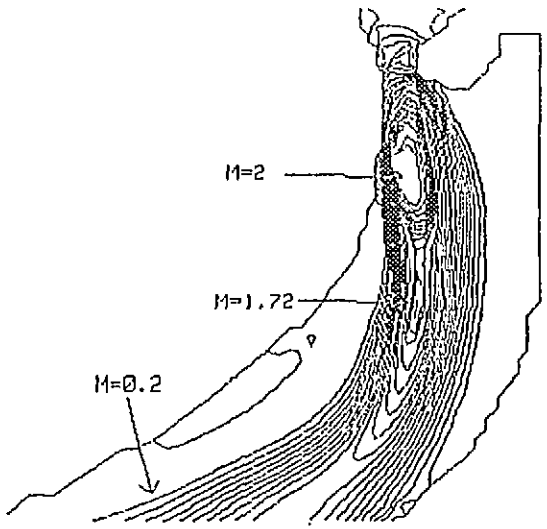

Fig 10 : Mach number (expansion rate=6)

2D MOCK-UP OF A GOVERNING VALVE
comparaison between Numerical and Experimental results
expansion ratio = 2.5

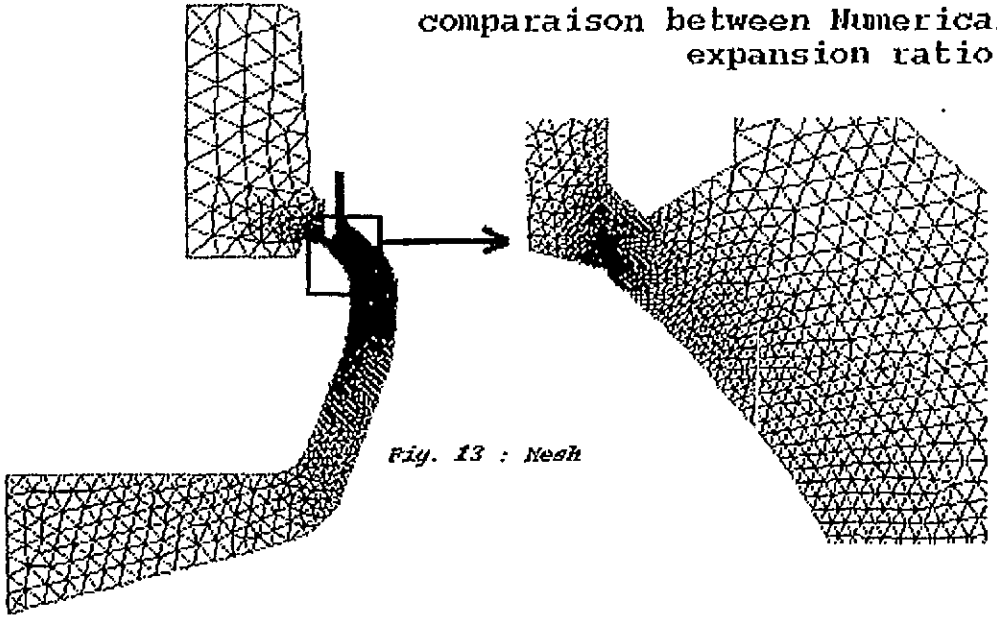

Fig. 13 : Mesh

Fig. 17 : schlieren photograph

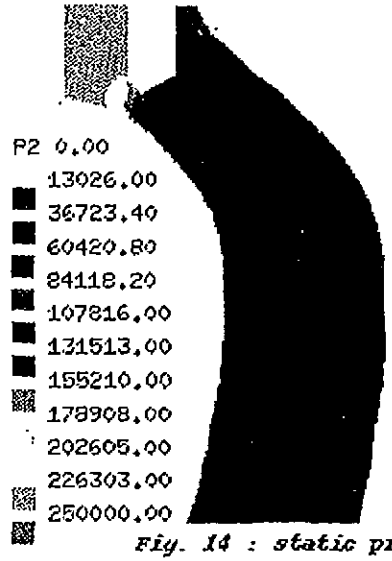

Fig. 14 : static pressure

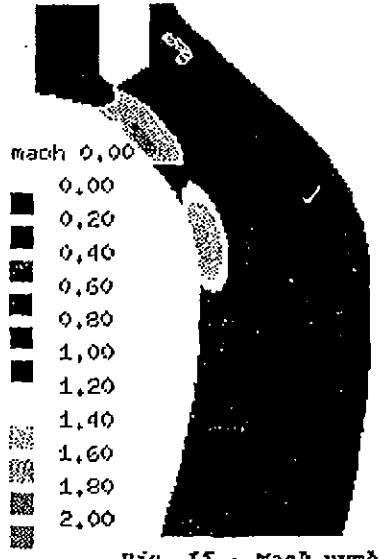

Fig. 15 : Mach number

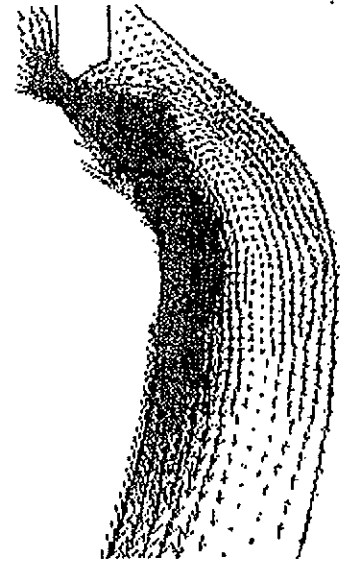

Fig. 16 : velocities

EDF
Electricité de France

Direction des Etudes et Recherches

Service Information Prospective et Normalisation

Département Systèmes d'information et de documentation

Groupe Exploitation de la Documentation Automatisée

1, avenue du Gal de Gaulle
92141 CLAMART Cedex
tel : 47 65 56 33

CLAMART Le 02/06/95

CEA
MIST/SBDS/SPRI
CENTRE DE SACLAY

91191 GIF SUR YVETTE CEDEX

à l'attention de :

MEMOIRE TECHNIQUE ELECTRONIQUE

****
Cette feuille est détachable grâce à la microperforation sur le coté droit.
****

Référence de la demande : **F528186** Votre commande :
Origine : **CATALOGUE DES NOTES DER**

Numéro du document : **95NB00017**

Titre : **EXTENSION DES ALGORITHMES POUR ECOULEMENTS INCOMPRESSIBLES AU COULEMENTS COMPRESSIBLES : VALIDATION SUR UNE MAQUETTE DE VANNE REGULATRICE**

Auteurs : **BARON F./CARUSO A./DUPLEX J./LEFEVRE L.**

Source : **COLL. NOTES INTERNES DER. PRODUCTION D'ENERGIE (HYDRAULIQUE, THE**
Serial :

Référence du document : **SANS**

Nombre de pages: **0011** Nombre d'exemplaires : **001** Support : **P**